X-ray resonant Raman scattering in the rare earths

Michel van Veenendaal, Paolo Carra, and B. T. Thole*
European Synchrotron Radiation Facility, Boîte Postale 220, F-38043 Grenoble Cédex, France
(Received 12 March 1996)

This paper develops a theory of resonant Raman scattering within the framework of a localized model. Expressions for the scattering amplitude and cross section are derived by employing the methods of spherical-tensor analysis; a simple factorization is obtained for the geometrical (angular dependence) and electronic (matrix element) components, which can therefore be studied independently. Photon polarization effects are examined. It is shown that, for fast collisions, the integrated intensity is expressible by way of spin and orbital effective operators, thus allowing for a simple interpretation of the scattering process. For the $2p \rightarrow 4f$, $3d \rightarrow 2p$ resonance in Gd^{3+}, Dy^{3+}, Ho^{3+}, and Er^{3+}, numerical calculations of the cross section are discussed. In the case gadolinium, the agreement between calculations and experiments provides further evidence for the quadrupolar nature of certain spectral features. [S0163-1829(96)05046-1]

I. INTRODUCTION

In the absence of an *ab initio* technique able to account for the full electron-electron interaction, the determination of the electronic structure in rare-earth systems has been approached from two opposite limits. As shown by inverse photoemission[1] and $3d$ x-ray absorption[2] data, the localized $4f$ electrons are well described by atomic, full-multiplet theory. An atomic framework is, however, inappropriate for describing the broad $5d$ band, and cannot explain the itinerant magnetism in a large number of rare-earth compounds. For these delocalized, largely unoccupied states, which are responsible for the interaction between the local $4f$ moments, a suitable theoretical description is provided by spin-polarized band-structure calculations, where exchange and correlation are treated within the local density approximation (density functional theory). For the $4f$ electronic states in rare-earth-containing materials this approximation is inadequate.[3]

Experimental information about the $5d$ states can be gathered through $2p$ x-ray absorption spectroscopy (XAS).[4] The corresponding spectra have, in general, an electric multipole character, with the above-edge structure assigned to dipolar transitions to the $5d$ band, and the pre-edge features ascribed to quadrupolar transitions to the narrow $4f$ states.[5–8] As the spectral resolution is rather broad, reflecting the short lifetime of the core excitation, it is difficult to fully disentangle the pre-edge structure from the remaining part of the spectrum.

Attempts have been made to overcome such a broadening by performing absorption-followed-by-emission experiments, considered as a single process: x-ray resonant Raman scattering (XRRS).[9] Notice that in this case the total electron or fluorescence yield is not measured. Only the energy of the photon in a single emission channel (the decay to a shallower core-hole final state) is detected, and narrower features are indeed observed. These do not stem, however, from a sharpening of the absorption process; instead, they are seen to arise from the structure of the final states, where the long lifetime of the shallow core hole results in a small spectral broadening.[10]

Upon tuning across the XRRS transferred energy, the $4f$ and $5d$ spectra appear clearly separated, a valuable feature in the study of the electronic structure of rare-earth systems. However, its full exploitation requires setting up a solid theoretical framework for XRRS, aimed at interpreting two general aspects of core-level spectroscopy: integrated intensities and spectral line shapes.

As shown for x-ray absorption and dichroism, a symmetry analysis of integrated intensities results in powerful sum rules,[11,12] relating the integral of the spectra, over a spin-orbit split edge, to the ground-state expectation value of spin and orbital coupled-tensor operators. When the scattering is fast, i.e., when the core-hole propagation in the intermediate state can be neglected, a similar coupled-tensor expansion for XRRS can be derived. The scattering is formally equivalent to an absorption process, in this case.

The importance of a proper determination of the spectral line shapes is not superseded by the amount of information contained in the integrated spectra: We have to make certain of the nature of the spectrum, for a correct application of the sum rules; as observed, $2p$ magnetic circular dichroism cannot simply be explained on the basis of electric dipolar transitions.

By resorting to the methods of spherical-tensor analysis, in the context of a single-ion picture, this paper develops a theory of XRRS. Technically, the derivation is laborious, as we are dealing with a two-photon process. Angular-momentum-recoupling techniques are employed to determine the symmetry (therefore the nature) of the cross section, as a function of photon polarization and scattering geometry. It is hoped that the reader with insufficient background will still be able to grasp the general lines of the work, omitting the algebraic details.

The outline of the paper is as follows. General expressions for the scattering amplitude and cross section are derived in Sec. II, with the special case of isotropic radiation treated in detail. Sec. III dicusses the fast-collision approximation and reports a numerical estimate of its range of applicability. Accurate numerical calculations for Gd^{3+}, Dy^{3+}, Ho^{3+}, and Er^{3+} are expounded in Sec. IV, where a comparision between analytical results and experimental

data is also made. Section V contains our concluding remarks.

Part of this work has previously been published.[10]

II. THEORETICAL FRAMEWORK

A. XRRS scattering amplitude

In a rare-earth ion, XRRS proceeds from the excitation of electric dipole and quadrupole transitions. An appropriate description of the process is obtained by expanding the $\mathbf{p}\cdot\mathbf{A}$ interaction between electrons and x rays into Bessel functions and spherical harmonics: $\mathbf{p}\cdot\boldsymbol{\epsilon} g_l(kr)\Sigma_m Y^l_m(\hat{\mathbf{k}})Y^l_m(\hat{\mathbf{r}})$. Here, $\boldsymbol{\epsilon}$ and $\hat{\mathbf{k}}$ denote the polarization and a unit vector in the direction of the photon momentum of the photon, respectively. Recoupling $\mathbf{p}$ and $Y^l_m(\hat{\mathbf{r}})$ to a total L results in the term

$$[[\boldsymbol{\epsilon}, Y^l_m(\hat{\mathbf{k}})]^L[\mathbf{p}, Y^l_m(\hat{\mathbf{r}})]^L]^0 g_l(kr), \tag{1}$$

with the couplings defined via Clebsch-Gordan coefficients

$$[A^{l'}, B^{l''}]^l_m \equiv \sum_{m'm''} C^{lm}_{l'm';l''m''} A^{l'}_{m'} B^{l''}_{m''}. \tag{2}$$

In the limit $kr \ll 1$, the value $l = L-1$ yields the largest contribution; this term can be rewritten as

$$[\mathbf{p}, Y^{L-1}(\hat{\mathbf{r}})]^L_M r^{L-1} = \frac{1}{\sqrt{L(2L+1)}} \mathbf{p}\cdot\boldsymbol{\nabla}(r^L Y^L_M), \tag{3}$$

so that

$$\langle\psi_2|\mathbf{p}\cdot\mathbf{A}+\mathbf{A}\cdot\mathbf{p}|\psi_1\rangle \sim \frac{2m(E_2-E_1)}{i\hbar\sqrt{L(2L+1)}}\langle\psi_2|r^L Y^L_M(\hat{\mathbf{r}})|\psi_1\rangle,$$

displaying the familiar electric multipole matrix element.

In this formulation, the x-ray XRRS amplitude $f_{L,L'}$ can be written as

$$f_{L,L'} = 4\pi\lambda\sum_z \sum_{\zeta=-z}^{z} T^{(z)*}_\zeta(\boldsymbol{\epsilon},\mathbf{k},\boldsymbol{\epsilon}'^*,\mathbf{k}') \times\langle f|F^{(z)}_\zeta(L,\lambda,L',\lambda')|g\rangle, \tag{4}$$

that is, as a linear combination of pairs of tensors of increasing rank z; here, $\lambda = |\mathbf{k}|^{-1}$. Each pair consists of an angular factor and of a frequency-dependent transition operator. The angular factor, determined by photon polarizations and wave vectors, is given by

$$T^{(z)*}_\zeta(L,L') = \sum_{M,M'} C^{z\zeta}_{L'M';LM}[\boldsymbol{\epsilon}\cdot\mathbf{Y}^*_{LM}(\hat{\mathbf{k}})] \times[\boldsymbol{\epsilon}'^*\cdot\mathbf{Y}_{L'M'}(\hat{\mathbf{k}}')],$$

with $\mathbf{Y}_{LM}(\hat{\mathbf{k}})$ a vector spherical harmonic of electric type.[13] In the second quantization formalism, the frequency-dependent transition operator takes the form

$$F^{(z)}_\zeta(L,\lambda,L',\lambda') = R^{L',\lambda'}_{L\lambda}(c_1,l;c_2,c_1) \sum_{l_z,\sigma,\text{all}\ m} S^{(z)}_\zeta \times(L,L')c^\dagger_{j_1m_1'}c_{j_2m_2}G(\omega_{\mathbf{k}})l^\dagger_{l_z\sigma}c_{j_1m_1}, \tag{5}$$

with

$$G(\omega_{\mathbf{k}}) = \sum_n \frac{|n\rangle\langle n|}{E_g+\hbar\omega_{\mathbf{k}}-E_n+i\Gamma_n/2} \tag{6}$$

and $\omega_{\mathbf{k}}$ the energy of the ingoing photon. Also,

$$R^{L',\lambda'}_{L,\lambda}(c_1,l;c_2,c_1) = K(c_1,L,l,\lambda)K(c_2,L',c_1,\lambda') \times\langle R_{n_1c_1j_1}(r)|r^{L'}|R_{n_2c_2j_2}(r)\rangle \times\langle R_{nl}(r)|r^L|R_{n_1c_1j_1}(r)\rangle,$$

with

$$K(c,L,l,\lambda) = -\frac{e}{\lambda^{L+1/2}} i^L \frac{C^{l0}_{c0;L0}}{(2L+1)!!} \times\left[\frac{(2c+1)(2L+1)(L+1)}{L(2l+1)}\right]^{1/2}$$

and $\langle R_{ncj}(r)|r^L|R_{n'c'j'}(r)\rangle$ the radial matrix element.

The angular dependence of the transition operator $S^{(z)}_\zeta(L,L')$ is given by

$$S^{(z)}_\zeta(L,L') = \sum_{\substack{M,M'\\ \gamma_1\gamma_2\gamma_1'\sigma'}} C^{z\zeta}_{L'M';LM}(-)^{L'-M'} C^{j_1m_1'}_{c_1\gamma_1';\frac{1}{2}\sigma'} \times C^{j_2m_2}_{c_2\gamma_2;\sigma'/2} C^{j_1m_1}_{c_1\gamma_1;\frac{1}{2}\sigma} C^{c_1\gamma_1'}_{c_2\gamma_2;L'-M'} C^{ll_z}_{c_1\gamma_1;LM}. \tag{7}$$

In these expressions, the operators $c_{j_1m_1}$ and $c_{j_2m_2}$ create a core hole in the intermediate and final states, respectively; $l^\dagger_{l_z\sigma}$ denotes the creation operator for outer-shell electrons. Core electrons are denoted by spin-orbit coupled quantum numbers ($j_i = c_i \pm \frac{1}{2}$, $i=1,2$); outer-shell electrons are labeled by uncoupled orbitals. The intermediate states $|n\rangle$ are eigenstates of the Hamiltonian of the system with energy E_n; they are assumed to be of the form $|n\rangle = \Sigma_{l_z\sigma m_1} a_{l_z\sigma m_1} l^\dagger_{\lambda\sigma} c_{j_1m_1}|g\rangle$. This amounts to neglecting many core-hole decay processes, e.g., nonradiative (Auger) decays, which might occur before the core hole (j_1) is filled by a core electron (j_2). In order not completely to disregard these events, a finite width $\Gamma \cong \pi\rho|V_A|^2$, with V_A the Auger matrix element and ρ the density of states in the continuum, has been introduced. The final states $|f\rangle$ differ from the initial one $|g\rangle$ by the presence of a particle-hole excitation. Figure 1 provides a schematic (one electron) picture of the resonance.

When the scattering is fast, so that photon absorption and emission are practically simultaneous, the energy dispersion of the intermediate state can be neglected;[17,18] this amounts to replacing $G(\omega_{\mathbf{k}})$ with

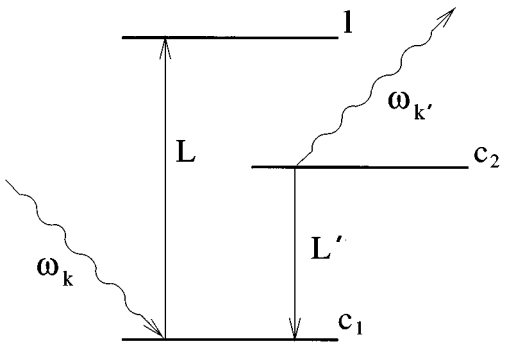

FIG. 1. One-electron picture of a resonant Raman process. Normally, in a rare-earth ion $c_1=2p$, $c_2=3d$, and $l=4f$.

$$\overline{G(\omega_{\mathbf{k}})}=\frac{1}{E_g+\hbar\omega_{\mathbf{k}}-\overline{E_n}+i\overline{\Gamma_n}/2},$$

with $\overline{E_n}$ the ''central'' energy of the transition and $\overline{\Gamma_n}$ its corresponding width. As a result, the j_1 core hole drops out (no propagation) of the amplitude

$$\langle f|c^{\dagger}_{j_1m_1'}c_{j_2m_2}l^{\dagger}_{l_z\sigma}c_{j_1m_1}|g\rangle=\delta_{m_1,m_1'}\langle f|c_{j_2m_2}l^{\dagger}_{l_z\sigma}|g\rangle. \quad (8)$$

More insight into the nature of the scattering process is obtained by rewriting expression (7) by use of standard techniques of angular momentum theory.[14,15] Given the relations

$$(-1)^{L'-M'}[j_1j_2c_1]^{-1/2}\sum_{\gamma_1'\sigma'\gamma_2}C^{j_1m_1}_{c_1\gamma_1';\frac{1}{2}\sigma'}C^{j_2m_2}_{c_2\gamma_2;\frac{1}{2}\sigma'}\times C^{c_1\gamma_1'}_{c_2\gamma_2;L'-M'}=(-1)^{c_1+m_1-1/2}\begin{pmatrix} j_1 & j_2 & L' \\ -m_1 & m_2 & -M'\end{pmatrix}\times\begin{Bmatrix} j_1 & j_2 & L' \\ c_2 & c_1 & \frac{1}{2}\end{Bmatrix} \quad (9)$$

and

$$\sum_{\xi}C^{a'\alpha'}_{x\xi;b'\beta'}C^{b\beta}_{x\xi;a\alpha}=(-1)^{b+\beta+b'-\beta'}[a'b]^{1/2}\times\sum_{y\eta}(-1)^{y-\eta}[y]\times\begin{pmatrix} a & a' & y \\ -\alpha & -\alpha' & -\eta\end{pmatrix}\times\begin{pmatrix} y & b' & b \\ -\eta & \beta' & \beta\end{pmatrix}\begin{Bmatrix} b & b' & y \\ a' & a & x\end{Bmatrix}, \quad (10)$$

we find

$$S^{(z)}_{\zeta}(L,L')=(-1)^{j_1+j_2+1}[j_1][j_2c_1zl]^{1/2}\begin{Bmatrix} j_1 & j_2 & L' \\ c_2 & c_1 & \frac{1}{2}\end{Bmatrix}\times\sum_{jm}[j]\begin{Bmatrix} j_1 & j & L \\ l & c_1 & \frac{1}{2}\end{Bmatrix}\begin{Bmatrix} L & L' & z \\ j_2 & j & j_1\end{Bmatrix}\times\begin{pmatrix} \frac{1}{2} & l & j \\ \sigma & l_z & -m\end{pmatrix}\begin{pmatrix} j & z & j_2 \\ m & -\zeta & -m_2\end{pmatrix}, \quad (11)$$

where the notation $[a\cdots b]=(2a+1)\cdots(2b+1)$ has been employed.

The recoupled form of $S^{(z)}(L,L')$ [the reader should pay attention to the last $3j$ symbol in expression (11)] provides a simple interpretation of the scattering process: When the scattering is fast, XRRS amounts to an effective 2^z-pole absorption from the core level j_2m_2 to the valence empty state $(l\frac{1}{2})jm$. Notice that, in this case, the transition operator is not purely orbital; it also depends on spin, as the spin-orbit interaction in the intermediate state allows for spin transitions, even in the absence of spin-orbit coupling in the ground and final states.

B. XRRS cross section for fast collisions

In the fast collision approximation, the coupled-multipolar expansion leads to the following form for the double-differential scattering cross section ($\hbar=1$):

$$\frac{d^2\sigma}{d\Omega_{\mathbf{k}'}d\hbar\omega_{\mathbf{k}'}}=8\pi\mathcal{K}^2\int_{-\infty}^{\infty}dt\ \ e^{i(\omega_{\mathbf{k}}-\omega_{\mathbf{k}'})t}\times\sum_{r\rho}\sum_{zz'}\mathcal{T}^{(zz')r*}_{\rho}\langle g|\mathcal{O}^{(zz')r}_{\rho}(t)|g\rangle, \quad (12)$$

with the geometrical factor $\mathcal{T}^{(zz')r}_{\rho}$ given by

$$\mathcal{T}^{(zz')r}_{\rho}=\sum_{\zeta\zeta'}C^{r\rho}_{z\zeta;z'\zeta'}T^{z}_{\zeta}T^{z'}_{\zeta'}. \quad (13)$$

The scattering operator can be written as

$$\mathcal{O}^{(zz')r}_{\rho}(t)=|\mathcal{A}^{L',\mathcal{K}'}_{L,\mathcal{K}}(\omega_{\mathbf{k}})|^2\sum_{\zeta\zeta'}C^{r\rho}_{z\zeta;z'\zeta'}\times\sum_{\substack{l_zl_z'\sigma\sigma'\\ m_1m_1'm_2m_2'}}S^{(z)\dagger}_{\zeta}S^{(z')}_{\zeta'}c^{\dagger}_{j_2m_2'}(t)l_{l_z'\sigma'}(t)l^{\dagger}_{l_z\sigma}c_{j_2m_2}. \quad (14)$$

The quantity

$$\mathcal{A}^{L',\mathcal{K}'}_{L,\mathcal{K}}(\omega_{\mathbf{k}})=\overline{G(\omega_{\mathbf{k}})}R^{L',\mathcal{K}'}_{L,\mathcal{K}}$$

denotes a dimensionless reduced scattering amplitude.

As observed, Eq. (11) describes an absorption process, induced by an effective photon of energy $\omega_{\mathbf{k}}-\omega_{\mathbf{k}'}$. Integrating over $\omega_{\mathbf{k}'}$, i.e., summing over the final states allowed by energy conservation, leads to an expansion for the integrated cross section in terms of coupled-tensor operators, formally

equivalent to the sum rule analysis for x-ray absorption and dichroism.[11,12] In view of the following discussion, the expansion is best performed by working with each photon coupled to itself. [Equation (12) employs an alternative formulation, with ingoing and outgoing photons coupled together.] This amounts to a redefinition of the geometry factors:

$$\mathcal{T}_\rho^{(zz')r}\rightarrow\widetilde{\mathcal{T}}_\rho^{(zz')r}=\sum_{\zeta\zeta'} C^{r\rho}_{z-\zeta;z'-\zeta'}\widetilde{T}^z_\zeta(L)\widetilde{T}^{z'}_{\zeta'}(L'),$$

with

$$\widetilde{T}^z_\zeta(L)=\sum_{M,M'} C^{z\zeta}_{LM';LM}[\boldsymbol{\epsilon}\cdot\mathbf{Y}^*_{LM}(\hat{\mathbf{k}})][\boldsymbol{\epsilon}^*\cdot\mathbf{Y}_{LM'}(\hat{\mathbf{k}})].$$

The scattering operator is transformed accordingly: $\mathcal{O}_\rho^{(zz')r}\rightarrow\mathcal{O}_\rho^{(zz')r}$. We find

$$\frac{d\sigma}{d\Omega_{\mathbf{k}'}}\cong 8\pi\lambda';^2\sum_{zz'r\rho}\widetilde{\mathcal{T}}_\rho^{(zz')r*}(L,L')\langle\mathcal{O}_\rho^{(zz')r}(0)\rangle, \quad (15)$$

with

$$\mathcal{O}_0^{(zz')r}(t)=|\mathcal{A}^{L',\lambda'}_{L,\lambda}(\omega_{\mathbf{k}})|^2\sum_{\zeta\zeta'} C^{r0}_{z\zeta;z'\zeta'}\times\sum_{\substack{\lambda\lambda'\sigma\sigma'\\ m_1m_1'm_2}} S^{(z)\dagger}_\zeta S^{(z')}_{\zeta'} l_{l_z'\sigma'}(t)l^\dagger_{l_z\sigma}; \quad (16)$$

here, the brackets $\langle\cdots\rangle$ are a shorthand for the ground-state expectation value.

Consider the absorptive part of the scattering operator

$$S^{(z)}_\zeta=\sum_{\substack{\gamma_1\gamma_1'\\ MM'''}} C^{z\zeta}_{LM;LM'''}C^{j_1m_1'}_{c_1\gamma_1';\frac{1}{2}\sigma'}C^{c_1\gamma_1'}_{ll_z';L-M'''}\times C^{j_1-m_1}_{c_1-\gamma_1;\frac{1}{2}-\sigma}C^{ll_z}_{c_1\gamma_1;LM}. \quad (17)$$

By applying the Wigner-Eckart theorem, and recoupling with use of the identity

$$\sum_{mm'} C^{jm'}_{a\alpha';b\beta'}C^{j-m}_{a-\alpha;b-\beta}\begin{pmatrix} j & j & z\\ m' & -m & -\zeta\end{pmatrix}=[j]\sum_{\substack{x\xi\\ y\eta}}(-1)^{x-\xi+y-\eta}[xy]\begin{pmatrix} a & a & x\\ \alpha' & -\alpha & \xi\end{pmatrix}\times\begin{pmatrix} x & z & y\\ -\xi & \zeta & \eta\end{pmatrix}\begin{pmatrix} y & b & b\\ -\eta & \beta & -\beta\end{pmatrix}\begin{Bmatrix} a & b & j\\ a & b & j\\ x & y & z\end{Bmatrix}, \quad (18)$$

followed by Eq. (10), we find

$$\sum_{\substack{\lambda\lambda'\sigma\sigma'm_1m_1'\\ \zeta\zeta'}} C^{r\rho}_{z\zeta;z'\zeta'}S^{(z)}_\zeta(L)C^{z'\zeta'}_{j_1m_1'j_1-m_1}n^{-1}_{j_1z'}l_{l_z'\sigma'}l^\dagger_{l_z\sigma}=\sum_{ab}\mathcal{C}^{abrzz'}_{j_1}(c_1,L,l)w^{(ab)r}_\rho n_{Lz}n^{-1}_{zz'r}\frac{[zz']^{1/2}}{[c_1lr]^{1/2}}, \quad (19)$$

where

$$\mathcal{C}^{abrzz'}_{j_1}(c_1,L,l)=\sum_x[j_1c_1labrx]\begin{Bmatrix} a & b & r\\ z & z' & x\end{Bmatrix}\times\begin{Bmatrix} c_1 & \frac{1}{2} & j_1\\ c_1 & \frac{1}{2} & j_1\\ x & b & z'\end{Bmatrix}\times\begin{Bmatrix} L & l & c_1\\ L & l & c_1\\ z & a & x\end{Bmatrix}n_{la}n_{sb}n_{abr}n^{-1}_{Lz}n^{-1}_{j_1z'}n_{zz'r}. \quad (20)$$

In a similar way, the emitting part of the scattering operator

$$S^{(z')}_{\zeta'}=\sum_{M',M''}C^{z'\zeta'}_{L'M';L'M''}[j_1j_2c_1c_2]^{1/2}\times\begin{Bmatrix} j_1 & j_2 & L'\\ c_2 & c_1 & \frac{1}{2}\end{Bmatrix}^2 C^{j_2-m_2}_{L'M';j_1-m_1}C^{j_1-m_1'}_{L'M'';j_2-m_2} \quad (21)$$

yields

$$\sum_{m_2}S^{(z')}_{\zeta'}(L')=\mathcal{B}^{z'}_{j_1j_2}(c_1L'c_2)C^{z'\zeta'}_{j_1m_1'j_1-m_1}\frac{n_{L'z'}}{[c_1c_2]^{1/2}n_{j_1z'}}, \quad (22)$$

with

$$\mathcal{B}^{z'}_{j_1j_2}(c_1,L',c_2)=(-1)^{j_1+j_2+c_1+c_2}[j_1j_2c_1c_2]\times\begin{Bmatrix} j_1 & j_2 & L'\\ c_2 & c_1 & \frac{1}{2}\end{Bmatrix}^2\begin{Bmatrix} L' & L' & z'\\ j_1 & j_1 & j_2\end{Bmatrix}\times n_{j_1z'}n^{-1}_{L'z'}. \quad (23)$$

The normalizing factors

$$n_{st}=\begin{pmatrix} s & t & s\\ -s & 0 & s\end{pmatrix}=\frac{(2s)!}{\sqrt{(2s-1)!(2s+t+1)!}} \quad (24)$$

and

$$n_{stu}=\begin{pmatrix} s & t & u\\ 0 & 0 & 0\end{pmatrix} \quad (25)$$

have been introduced to obtain rational expressions for the coefficients $\mathcal{B}^{z'}_{j_1 j_2}(c_1,L',c_2)$ and $\mathcal{C}^{abrzz'}_{j_1}(c_1,L,l)$.

The previous results lead to the following form for the scattering operator:

$$\mathcal{O}^{(zz')r}_{\rho}(0)=|\mathcal{A}^{L',\lambda'}_{L,\lambda}(\omega_{\mathbf{k}})|^2\sum_{ab}\mathcal{C}^{abrzz'}_{j_1}(c_1,L,l)w^{(ab)r}_{\rho}\mathcal{B}^{z'}_{j_1 j_2}\times(c_1,L',c_2)n_{Lz}n_{L'z'}n^{-1}_{zz'r}\frac{[zz']^{1/2}}{[lc_1^2c_2r]^{1/2}}. \quad (26)$$

This is our main analytical result for a $j_1 j_2$ resonance. Inserted into Eq. (15), it yields the XRRS cross section, integrated over $\omega_{\mathbf{k}'}$, as the ground-state expectation of a linear combination double-tensor operators $\langle w^{(ab)r}\rangle$. These tensors describe the multipole moments of the charge and magnetic distribution of the valence l electrons. The indexes a and b denote the orbital and spin parts, respectively; their values are limited to $a=0,\ldots,2l$ and $b=0,1$, because of the triads (l,l,a), and $(\frac{1}{2},\frac{1}{2},b)$. For $b=0$, the operators are purely orbital; for $b=1$, they depend on spin.

The relation between double tensors and second-quantization operators has been established by Judd[16] through the relation

$$W^{(ab)r}_{\rho}=-\sum_{\substack{l_z l'_z,\sigma\sigma'\\ \alpha\beta}} C^{r\rho}_{a-\alpha;b-\beta}C^{a\alpha}_{l'_z;l_z}C^{b\beta}_{\frac{1}{2}\sigma';\frac{1}{2}\sigma}l_{l'_z\sigma'}l^{\dagger}_{l_z\sigma}; \quad (27)$$

his formalism has been applied to XAS spectroscopy,[11,12] x-ray anomalous scattering,[17,18] and photoemission.[19] In the present work we employ rescaled coupled-tensor operators, defined by[20,21]

$$w^{(ab)r}_{\rho}=(-1)^{a-b+r}[abr]^{-1/2}n^{-1}_{la}n^{-1}_{sb}n^{-1}_{abr}W^{(ab)r}_{\rho}, \quad (28)$$

to remove the normalization of the Clebsch-Gordan coefficients. This normalization is irrelevant when dealing with the physical operators, that is, the coupled tensors $W^{(ab)r}_{\rho}$ expressed in terms of elementary spin and orbital operators.[16,22] (Examples of physical operators are provided by

$$n_h=w^{000}_0 \quad \text{(number of holes)},$$

$$L_{\xi}=-r_{l1}r_{s0}w^{101}_{\xi}=-lw^{101}_{\xi} \quad \text{(orbital momentum)},$$

$$S_{\eta}=-r_{l0}r_{s1}w^{011}_{\eta}=-sw^{011}_{\eta} \quad \text{(spin)},$$

$$\mathbf{L}\cdot\mathbf{S}=r_{l1}r_{s1}w^{110}_0=lsw^{110}_0 \quad \text{(spin orbit)}.$$

Similar identities can be obtained for higher-rank tensors.) Expressions (27) and (28) define coupled-tensor operators for the valence empty states (holes).

The scaling factor

$$n^{zz'r}(c_1LlL'c_2)=n_{Lz}n_{L'z'}n^{-1}_{zz'r}\frac{[zz']^{1/2}}{[lc_1^2c_2r]^{1/2}}, \quad (29)$$

arising from the normalization constants, can be conveniently absorbed into the angular dependence; this is achieved by redefining the cross section in terms of $\overline{\mathcal{T}}^{(zz')r}=\widetilde{\mathcal{T}}^{(zz')r}n^{zz'r}$ and $\overline{\mathcal{O}}^{(zz')r}=\widetilde{\mathcal{O}}^{(zz')r}/n^{zz'r}$. In this way, a simple and transparent factorization of the scattering operator

$$\langle\overline{\mathcal{O}}^{(zz')r}_{\rho}(0)\rangle=|\mathcal{A}^{L',\lambda'}_{L,\lambda}(\omega_{\mathbf{k}})|^2\mathcal{B}^{z'}_{j_1 j_2}(c_1,L',c_2)\sum_{ab}\mathcal{C}^{abrzz'}_{j_1}\times(c_1,L,l)\langle w^{(ab)r}_{\rho}\rangle. \quad (30)$$

is obtained.

As for the amplitude [see Eq. (3) and ensuing discussion], the coupled-multipolar expansion yields the scattering cross section as a linear combination of pairs of tensors of increasing rank r, which transform according to the irreducibile representations of the spherical group (SO_3). Consider $\langle\overline{\mathcal{O}}^{(zz')r}_{\rho}\rangle$ and keep in mind that, to yield a nonzero value, the operator $\mathcal{O}^{(zz')r}$ has to be totally symmetric. In spherical symmetry only $r=0$ has such a property. In lower symmetry, also those $r>0$ tensors that branch to the totally symmetric representation will contribute to the scattering.

Specific examples will help clarify this point. The case of a magnetic system with negligible crystal fields amounts to considering the irreducibile representations of the cylindrical group; they are given by the group $(SO_3)\rightarrow$ subgroup (SO_2) branching: $r\rightarrow\rho=\{-r,\ldots,r\}$, with $\rho=0$ the totally symmetric representation. Only the linear combination

$$\sum_r\sum_{zz'}\overline{\mathcal{T}}^{(zz')r*}_0\langle\overline{\mathcal{O}}^{(zz')r}_0\rangle \quad (31)$$

will therefore contribute to the scattering cross section. This result can be generalized to any point-group symmetry, where the totally symmetric representations are usually denoted by A_1. (Details about this simple group-theoretical analysis of x-ray resonant scattering can be found in Ref. 23.) The remaining part of this work will be restricted to the case of SO_2 symmetry .

As pointed out, the linear combination

$$\sum_{ab}\mathcal{C}^{abrzz'}_{j_1}(c_1,L,l)\langle w^{(ab)r}_0\rangle$$

describes the excitation (absorption) process. The deexcitation (emission) process is governed by the factor $\mathcal{B}^{z'}_{j_1 j_2}(c_1,L',c_2)$, yielding the probability of detecting z'-polarized radiation emitted in the $j_2\rightarrow j_1$ decay.

The (most probable) $l=c_1+L$ transition results in simpler coefficients; we find

$$\mathcal{C}^{abrzz'}_{j_1^+}(c_1)=\sum_x[arx]\frac{[c_1]n^2_{c_1x}}{2n^2_{j_1^+z'}}\begin{Bmatrix}a & b & r\\ z & z' & x\end{Bmatrix}\times n_{xbz'}n_{zz'r}n_{abr}n_{xaz} \quad (32)$$

and

$$\mathcal{C}^{abrzz'}_{j_1^-}(c_1)=(-1)^{b\frac{1}{2}}[j_1^-ar]n^2_{abr}n^2_{zz'r}, \quad (33)$$

with $j_1^{\pm}=c_1\pm\frac{1}{2}$.

In the specific case of a $2p \rightarrow 4f$ absorption in cylindrical symmetry, the permitted terms $\Sigma_{ab} C_{j_1}^{abrzz'} \langle w_0^{(ab)r} \rangle$ are listed in Table I. Only the triads $(zz')r$ allowed by ingoing quadrupolar and outgoing dipolar radiation are included in the table.

For the coefficient $\mathcal{B}^{z'}_{j_1 j_2}(c_1, L', c_2)$, numerical values of interest are given in Table II. Notice that the $j_2 = \frac{5}{2} \rightarrow j_1 = \frac{1}{2}$ electronic transition is forbidden; owing to Coulomb mixing, the $L_2 M_5$ edge has, however, a small but finite intensity.

C. Isotropic outgoing photon

The expressions for the integrated intensities, which were derived in the previous section, are general. Most experiments are, however, performed without detecting the polarization of the outgoing beam. This is the case of an isotropic outgoing photon. It corresponds to setting $z' = 0$ in Eq. (26), implying $z = r$, and yielding

$$\langle \overline{\mathcal{O}_0^{(r0)r}}(0) \rangle = |\mathcal{A}_{L,\lambda}^{L',\lambda'}(\omega_{\mathbf{k}})|^2 \mathcal{B}^0_{j_1 j_2}(c_1, L', c_2) \sum_{ab} \mathcal{C}_{j_1}^{abrr0} \times (c_1, L, l) \langle w_0^{(ab)r} \rangle. \tag{34}$$

Restricting ourselves to the particular case $c_1 = l - L = c_2 - L'$, we rewrite the function $C_{j_1^{\pm}}^{abrr0}(c_1)$ as a product of two factors:

$$\mathcal{C}_{j_1^{\pm}}^{abrr0}(c_1) = M_b(j_1^{\pm}) N_{abr}. \tag{35}$$

Using the reduction formula given in Appendix A and the fact that $2[b] n_{sb}^2 = 1$, the functions $M_b(j_1^{\pm})$ can be given the form

$$M_b(j_1^+) = \tfrac{1}{2}[j_1^+ c_1] n_{c_1 b}^2$$

and

$$M_b(j_1^-) = (-)^b \tfrac{1}{2}[j_1^-],$$

so that

$$M_b(j_1^+) + M_b(j_1^-) = [c_1] \delta_{b,0}, \tag{36}$$

$$M_b(j_1^+) - \frac{c_1 + 1}{c_1} M_b(j_1^-) = [c_1] \delta_{b,1}. \tag{37}$$

Thus, adding the two partners of a spin-orbit split edge $(j_1^{\pm})$ provides the spin-independent part $(b = 0)$ of the integrated intensity; a ''weighted'' difference, Eq. (37), yields the spin-dependent $(b = 1)$ counterpart. The remaining factor N_{abr} is defined by

$$N_{abr} = [a] n_{abr}^2;$$

special cases of interest are

$$N_{r0r} = [r] n_{r0r}^2 = 1,$$

$$N_{r-1,1,r} = [r-1] n_{r-1,1,r}^2 = \frac{r}{[r]}, \tag{38}$$

TABLE I. The combinations $\Sigma_{ab} C_{j_1}^{abrzz'} \langle w^{abr} \rangle$ for the excitation of a $2p$ $(j_1 = \frac{3}{2}, \frac{1}{2})$ core hole into the $4f$ shell, as a function of r, z, z'. When $z + z' + r$ is odd, the values $\{[r]^2/([r]^2 - 1)\} w^{r1r}$ are tabulated.

rzz'	$j_1 = \frac{3}{2}$
000	$2w^{000} + w^{110}$
011	$\frac{1}{9}(5w^{000} + 4w^{110})$
022	$\frac{1}{5}(w^{000} + 2w^{110})$
101	$\frac{1}{9}(10w^{011} + 15w^{101} + 2w^{211})$
110	$\frac{1}{3}(w^{011} + 6w^{101} + 2w^{211})$
112	$\frac{2}{15}(5w^{011} + 3w^{101} + w^{211})$
121	$\frac{2}{45}(w^{011} + 15w^{101} + 11w^{211})$
132	$\frac{9}{35}(w^{101} + 2w^{211})$
202	$2w^{112} + w^{202}$
211	$\frac{2}{45}(17w^{112} + 25w^{202} + 3w^{312})$
220	$\frac{1}{5}(2w^{112} + 10w^{202} + 3w^{312})$
222	$\frac{2}{35}(7w^{112} + 5w^{202} + 3w^{312})$
231	$\frac{1}{35}(2w^{112} + 25w^{202} + 18w^{312})$
242	$\frac{2}{7}(w^{202} + 2w^{312})$
312	$\frac{3}{5}(2w^{213} + w^{303})$
321	$\frac{1}{35}(24w^{213} + 35w^{303} + 4w^{413})$
330	$\frac{1}{7}(3w^{213} + 14w^{303} + 4w^{413})$
332	$\frac{4}{105}(9w^{213} + 7w^{303} + 5w^{413})$
341	$\frac{4}{189}(3w^{213} + 35w^{303} + 25w^{413})$
422	$\frac{18}{35}(2w^{314} + w^{404})$
431	$\frac{4}{189}(31w^{314} + 45w^{404} + 5w^{514})$
440	$\frac{1}{9}(4w^{314} + 18w^{404} + 5w^{514})$
442	$\frac{20}{693}(11w^{314} + 9w^{404} + 7w^{514})$
532	$\frac{10}{21}(2w^{415} + w^{505})$
541	$\frac{5}{297}(38w^{415} + 55w^{505} + 6w^{615})$
543	$\frac{20}{1001}(26w^{415} + 7w^{615})$
642	$\frac{5}{11}(2w^{516} + w^{606})$
rzz'	$j_1 = \frac{1}{2}$
000	$w^{000} - w^{110}$
011	$\frac{1}{3}(w^{000} - w^{110})$
101	$\frac{1}{3}(-w^{011} + 3w^{101} - 2w^{211})$
110	$\frac{1}{3}(-w^{011} + 3w^{101} - 2w^{211})$
121	$\frac{2}{15}(-w^{011} + 3w^{101} - 2w^{211}))$
211	$\frac{2}{15}(-2w^{112} + 5w^{202} - 3w^{312})$
220	$\frac{1}{5}(-2w^{112} + 5w^{202} - 3w^{312})$
231	$\frac{3}{35}(-2w^{112} + 5w^{202} - 3w^{312})$
321	$\frac{3}{35}(-3w^{213} + 7w^{303} - 4w^{413})$
330	$\frac{1}{7}(-3w^{213} + 7w^{303} - 4w^{413})$
341	$\frac{4}{63}(-3w^{213} + 7w^{303} - 4w^{413})$
431	$\frac{4}{63}(-4w^{314} + 9w^{404} - 5w^{514})$
440	$\frac{1}{9}(-4w^{314} + 9w^{404} - 5w^{514})$
541	$\frac{5}{99}(-5w^{415} + 11w^{505} - 6w^{615})$

$$N_{r+1,1,r} = [r+1] n_{r+1,1,r}^2 = \frac{r+1}{[r]}.$$

In the case of outgoing isotropic radiation, the emission process, determined by

TABLE II. The coefficients $B^{z'}_{j_1 j_2}$ giving the probability of the decay of the z'-polarized $2p$-core hole ($j_1=\frac{3}{2},\frac{1}{2}$) by radiative decay of a $3d$-core electron ($j_2=\frac{5}{2},\frac{3}{2}$) into the $2p$ orbital.

j_1 z'	$j_2=\frac{3}{2}$	$j_2=\frac{5}{2}$
$\frac{1}{2}$ 0	5	0
$\frac{1}{2}$ 1	$\frac{5}{3}$	0
$\frac{1}{2}$ 2	0	0
$\frac{3}{2}$ 0	$\frac{1}{2}$	$\frac{9}{2}$
$\frac{3}{2}$ 1	$-\frac{1}{5}$	$\frac{27}{10}$
$\frac{3}{2}$ 2	$-\frac{2}{5}$	$\frac{9}{10}$

$$\mathcal{B}^0_{j_1 j_2}(c_1,L',c_2)=[c_1c_2j_2]\begin{Bmatrix} j_1 & j_2 & L' \\ c_2 & c_1 & \frac{1}{2}\end{Bmatrix}^2 \tag{39}$$

can only provide information about the number of holes, which are created in the absorption process with z-polarized radiation. Adding the two final-state edges yields

$$\sum_{j_2=j_2^+,j_2^-}\mathcal{B}^0_{j_1 j_2}(c_1,L',c_2)=[c_2]. \tag{40}$$

When $z'=0$, the multipolar expansion for the XRRS cross section is very similar to that obtainable for the absorption coefficient, in the x-ray region. In establishing this connection, it is convenient to normalize expression (34) to the total isotropic intensity, defined as

$$\begin{aligned}\langle\overline{\mathcal{O}}^{(00)0}_0\rangle&=\sum_{j_1 j_2}\langle\overline{\mathcal{O}}^{(00)0}_0(0,j_1,j_2)\rangle\\&=|\mathcal{A}^{L',\chi'}_{L,\chi}(\omega_{\mathbf{k}})|^2[c_1c_2]\langle n_h\rangle,\end{aligned} \tag{41}$$

where the sum runs over the pairs of partners j_1,j_2; we have

$$\langle\overline{O}^{(r0)r}_0(0,j_1,j_2)\rangle=\frac{\langle\overline{\mathcal{O}}^{(r0)r}_0(0,j_1,j_2)\rangle}{\langle\overline{\mathcal{O}}^{(00)0}_0\rangle}. \tag{42}$$

Spin-independent scattering is then described by

$$\langle\overline{O}^{(z0)z}(j_1^+)\rangle+\langle\overline{O}^{(z0)z}(j_1^-)\rangle=\frac{1}{\langle n_h\rangle}\langle w^{(z0)z}_0\rangle. \tag{43}$$

For the spin-dependent operators, we find

$$\begin{aligned}&\langle\overline{O}^{(z0)z}(j_1^+)\rangle-\frac{c_1+1}{c_1}\langle\overline{O}^{(z0)z}(j_1^-)\rangle\\&\quad=\frac{1}{\langle n_h\rangle}\left\{\frac{z}{[z]}\langle w^{(z-1,1)z}_0\rangle+\frac{z+1}{[z]}\langle w^{(z+1,1)z}_0\rangle\right\}.\end{aligned} \tag{44}$$

Experimentally, the excitations to the $4f$ shell and to the $5d$ band are separable only at the L_3M_5 edge, that is, for the $j_1^+j_2^+$ resonance.

At a given edge, the normalization to the isotropic spectrum is impractical, as

$$\begin{aligned}\langle\overline{\mathcal{O}}^{(00)0}_0(0,j_1^+,j_2^+)\rangle&=\mathcal{B}^0_{j_1^+j_2^+}(c_1,L',c_2)M_0(j_1^+)\\&\quad\times\left\{\langle w^{(00)0}_0\rangle+\frac{c_1}{c_1+1}\langle w^{(11)0}_0\rangle\right\},\end{aligned} \tag{45}$$

which contains the ground-state expectation value of the valence-band spin-orbit coupling, a quantity not so easy to determine experimentally. In this case, the unnormalized expansion of the scattering operator reads

$$\begin{aligned}\langle\overline{\mathcal{O}}^{(z0)z}_0(0,j_1^+,j_2^+)\rangle&=\mathcal{B}^0_{j_1^+j_2^+}(c_1,L',c_2)M_0(j_1^+)\\&\quad\times\left\{\langle w^{(z0)z}_0\rangle+\frac{c_1}{c_1+1}\right.\\&\quad\left.\times\left(\frac{z}{[z]}\langle w^{(z-1,1)z}_0\rangle+\frac{z+1}{[z]}\langle w^{(z+1,1)z}_0\rangle\right)\right\}.\end{aligned}$$

D. Isotropic ingoing photon

The case of an ingoing isotropic photon can be treated in a similar way. Setting $z=0$ in Eq. (30) yields

$$\begin{aligned}\langle\overline{\mathcal{O}}^{(0r)r}_0(0)\rangle&=|\mathcal{A}^{L',\chi'}_{L,\chi}(\omega_{\mathbf{k}})|^2(-1)^{j_1+j_2+c_1+c_2}\mathcal{B}^0_{j_1^+j_2^+}\\&\quad\times(c_1,L',c_2)\sum_{ab}M_a(j_1^+)N_{abr}\langle w^{(ab)r}_0\rangle.\end{aligned} \tag{46}$$

The appearance of $\mathcal{B}^0_{j_1^+j_2^+}$ and $M_a(j_1^+)$ follows from the reduction of the $6j$ symbol in Eq. (23) for $j_2^+=j_1^++L'$.

E. General XRRS cross section

The results reported so far, in this section, were derived for fast collisions. In the remaining part of the paper, this approximation will be often released, and the various components of the full scattered intensity,

$$\begin{aligned}I_{MM'}(\omega_{\mathbf{k}},\omega_{\mathbf{k}'})&=\sum_f\left|\sum_n\frac{\langle f|D^{(L')}_{M'}|n\rangle\langle n|D^{(L)}_M|g\rangle}{\hbar\omega_{\mathbf{k}}+E_g-E_n+i\Gamma_n/2}\right|^2\\&\quad\times\delta(\hbar\omega_{\mathbf{k}}+E_g-\hbar\omega_{\mathbf{k}'}-E_f),\end{aligned} \tag{47}$$

calculated by exact diagonalization. Here, $D^{(L)}_M$ denotes the components of the electric 2^L-pole operator. In this case, the coupled spectra for ingoing and outgoing isotropic photons are given by

$$I^{(0z)z}(\omega_{\mathbf{k}},\omega_{\mathbf{k}'})=\sum_{MM'}C^{z0}_{L'M';L'M'}I_{MM'}(\omega_{\mathbf{k}},\omega_{\mathbf{k}'}) \tag{48}$$

and

$$I^{(z0)z}(\omega_{\mathbf{k}},\omega_{\mathbf{k}'})=\sum_{MM'} C^{z0}_{LM;LM} I_{MM'}(\omega_{\mathbf{k}},\omega_{\mathbf{k}'}), \quad (49)$$

respectively.

III. FAST-COLLISION APPROXIMATION

This approximation amounts to neglecting the dispersion of the intermediate states; E_n and Γ_n can then be taken as constants, and the expansion for the resonant denominator,

$$\left(E_n-E_g-\hbar\omega-i\frac{\Gamma_n}{2}\right)^{-1} = \left(\overline{E_n}-E_g-\hbar\omega-i\frac{\overline{\Gamma_n}}{2}\right)^{-1} \times\sum_{k=0}^{\infty}\left(\frac{\overline{E_n}-i\overline{\Gamma_n}/2-E_n+i\Gamma_n/2}{\overline{E_n}-E_g-\hbar\omega-i\overline{\Gamma_n}/2}\right)^k, \quad (50)$$

truncated at $k=0$. Collisions are fast when

$$\mathrm{Max}(|\hbar\omega_1-E_n+E_g|,\Gamma_n)\gg D,$$

with $D=[\overline{(E_n-\overline{E_n})^2}]^{1/2}$ the energy spread of the intermediate states.

Put another way, the approximation guarantees full intermediate-state interference, a *sine qua non* in the derivation of the coupled-tensor expansion for the cross section. [Notice that, in general, $G(\omega)$ reduces such an interference for energy separations larger than Γ_n.]

For isotropic outgoing radiation, it can be shown that all interference terms $n\neq n'$ cancel out upon integration over the final states; the fast-collision approximation is exact in this case. Indeed, the emission matrix element, shorn of irrelevant factors, can be given the form

$$\langle n'|c^{\dagger}_{j_2m_2'}c_{j_1m_1'}|f\rangle\langle f|c^{\dagger}_{j_1m_1}c_{j_2m_2}|n\rangle \times\sum_{\substack{M'M''\\ m_1m_1',m_2m_2'}}(-1)^{j_1-m_1+j_2-m_2'-q_2-q_2'} \times\begin{pmatrix} j_1 & L' & j_2\\ -m_1 & M' & -m_2\end{pmatrix}\begin{pmatrix} j_2 & L' & j_1\\ -m_2' & M'' & m_1'\end{pmatrix} \times\begin{pmatrix} L' & L' & z'\\ M' & -M'' & \zeta'\end{pmatrix}. \quad (51)$$

Integrating over the final states sets $m_2=m_2'$, as no $3d$ core hole is present in the intermediate state. For $z'=0$, it then follows that $m_1=m_1'$, in the resulting expression. In turn, this implies that $|n\rangle=|n'\rangle$, leading to a cancellation of all interference effects. In this case, XRRS is equivalent to an x-ray absorption process.

For polarized outgoing radiation, an estimate of the error brought about by the fast-collision approximation can be obtained numerically. Consider the L_3M_5 edge in Ho^{3+} and Er^{3+}. The full intensities $I^{(0z)z}$, integrated over $\omega_{\mathbf{k}'}$, and for $z=1$ and 2, are shown in Fig. 2, as a function of the intermediate-state broadening in the range $0\leqslant\Gamma_n\leqslant 4.2$ eV. (The reduced scattering amplitude has been set to unity.) In the same figure, results for the special $\Gamma=\infty$ case (fast collisions in the presence of Coulomb mixing) are given by the intersections with the dashed vertical line I. A comparison with the fast-collision approximation neglecting Coulomb mixing, as from Eq. (46), is provided by the intersections with the dashed vertical line II. (Details about these numerical calculations will be given in the next section.)

IV. CALCULATED SPECTRA

As shown by a two-dimensional analysis of the cross section, plotted as a function of ingoing $\omega_{\mathbf{k}}$ and transferred $\omega_{\mathbf{k}}-\omega_{\mathbf{k}'}$ photon energies (see Figs. 3, 6, 8, and 10), XRRS can probe the rare-earth electronic structure in different ways.

A scan parallel to the $\omega_{\mathbf{k}}$ axis amounts to moving through the intermediate-state structure. The spectrum has resolution Γ_n, and is obtained by retaining only one final state, selected by the given energy transfer, in Eq. (47).

Along the $\omega_{\mathbf{k}}-\omega_{\mathbf{k}'}$ axis, the final-state structure is probed. In this case, the fixed ingoing energy selects a Γ_n-wide set of intermediate states. Notice that for systems with incomplete $4f$ and $5d$ shells, two groups of final states are scanned:[24] (i) the $3d^94f^{n+1}$ multiplet reached from the intermediate states $2p^54f^{n+1}$ and (ii) the $3d^94f^n5d^{m+1}$ final states reached from the $2p^54f^n5d^{m+1}$ intermediate states.

Scanning $\omega_{\mathbf{k}}$ while keeping $\omega_{\mathbf{k}'}$ fixed amounts to diagonally crossing the plot; a superposition of the full set of intermediate and final states is therefore recorded.[9]

Numerical calculations have been performed, with use of Cowan's Hartree-Fock and multiplet programs,[25] for a number of single rare-earth ions. Our results are restricted to the quadrupole $\rightarrow$ dipole part of the resonance, well described by atomic theory. All electric quadrupolar transitions from the Hund's rule ground state of the $|g\rangle=|2p^63d^{10}4f^n\rangle$ configuration to the full multiplet of the $|n\rangle=|2p^53d^{10}4f^{n+1}\rangle$ intermediate state were calculated and similarly for all electric dipolar transitions from the intermediate- to the final-state multiplet $|f\rangle=|2p^63d^94f^{n+1}\rangle$. Notice that the fast-collision approximation is not used in this case, as the intermediate state is determined by exact diagonalization. In the calculation, the Slater parameters F^k and G^k were reduced to 80% of their atomic value to account for intra-atomic screening. The absolute energy shifts were determined by matching the numerical spectra to the experimental data, as the calculated center-of-gravity energy is in error by a few eV. The ion symmetry was taken to be SO_2, that of a magnet with negligible crystal-field effects. (The branching $SO_3\supset SO_2$ was implemented using Butler's group-chain methods.[26])

To account for the finite lifetime of the final states, the energy-conservation δ function was broadened into a Lorentzian of width γ_f. The spectra shown here were obtained with $\Gamma_n=4$ eV and $\gamma_f=0.3$ eV.

A. Gadolinium

Circular magnetic x-ray dichroism spectra, at the $L_{2,3}$ edges of gadolinium metal, have been explained by taking

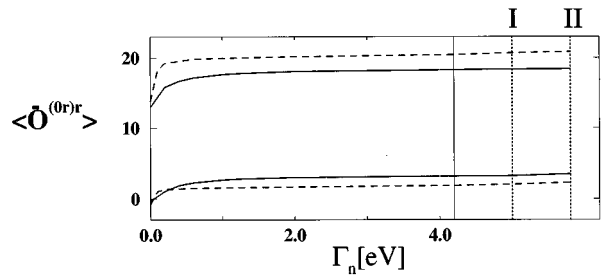

FIG. 2. The integrated $I^{(0z)z}$ for Er (solid line) and Ho (dashed line) obtained from exact diagonalization, in the range $0 \leqslant \Gamma_n \leqslant 4.2$. A comparison with the fast-collision approximation, with or without Coulomb interactions, is provided by the intersections with the vertical lines I and II, respectively.

into account dipolar transitions to the spin-polarized conduction bands, as well as quadrupole transitions to the highly localized $4f$ states. Quadrupolar transitions can appear below the absorption edge because of the strong Coulomb interaction (8–10 eV, in the solid) between the $4f$ electrons and the $2p$ core hole, in the final state. This amounts to considering the following configurations (in order of increasing energy): $|2p^5 4f^8 5d^0\rangle$ and $\alpha|2p^5 4f^7 5d^1\rangle + \beta|2p^5 4f^8 \underline{X} d^1\rangle$, where $\underline{X}$ denotes the hole density on neighboring sites that compensates the extra $4f$ electron. Notice that, even for absorption to the $5d$ orbitals, the $4f$ states are responsible for most of the core-hole screening. A screened Coulomb interaction of comparable strength, between the $3d$ hole and the $4f$ electrons, is also active in the XRRS final state. In this case, a scan parallel to $\omega_{\mathbf{k}} - \omega_{\mathbf{k}'}$ amounts to probing the $|3d^9 4f^8 5d^0\rangle$ and $\alpha'|3d^9 4f^7 5d^1\rangle + \beta'|3d^9 4f^8 \underline{X} d^1\rangle$ structures, with the narrow resolution of the $3d$ core hole. With respect to circular dichroism, XRRS affords therefore a clearer separation of $4f$ and $5d$ spectral features.

The calculated intensity $I^{(00)0}$ (unpolarized ingoing and outgoing photons) for the $L_3 \rightarrow M_5$ part of the spectrum is shown in Fig. 3, as a function of ingoing and transferred photon energy.

Figure 4 gives the dependence of the spectra on the polarization of the ingoing photon. We notice that only $I^{(10)1}$ has a significant integrated intensity. This behavior could have been inferred from an analysis of the coupled-tensor operators $w^{(ab)r}$. In LSJ coupling, the Gd^{3+} ($4f^7$) ground state is ${}^8S_{7/2}$, and all coupled tensor $w^{(ab)r}$, with the exception of $w^{(00)0} = n_h$ and $s w^{(01)1} = S_z$, are zero. In intermediate coupling, these vanishing operators acquire a finite, though small value. This implies that, apart from spin, polarization effects are negligible in Gd^{3+}. Notice that a vanishing integrated intensity does not necessarily imply a vanishing spectrum.

As a function of $\omega_{\mathbf{k}}$, gadolinium displays no spectral structure; just a Lorentzian variation of the intensity is recorded across the $2p \rightarrow 4f$ absorption edge. As shown in Fig. 4(a), the same behavior is observed in the integrated isotropic intensity, yielding a spectrum proportional to $2p \rightarrow 4f$ x-ray absorption. (A second peak, centered at 7250 eV, is also present in the integrated data; this feature should be ascribed to $2p \rightarrow 5d$ transitions.)

More spectral structure is present in the direction of the transferred energy axis. As $E_f - E_g = \omega_{\mathbf{k}} - \omega_{\mathbf{k}'}$, the transferred energy should be comparable to the $3d \rightarrow 4f$ absorption energy.

The fact that $3d \rightarrow 4f$ x-ray absorption and XRRS result in the same $3d^9 4f^{n+1}$ final-state configuration may lead one to believe that their spectral features are alike. This is not the case, in general; the matrix elements are different for the two spectroscopies (quadrupolar absorption followed by dipolar emission in XRRS and a single dipolar step in x-ray absorption), thus implying different selection rules and line shapes.

An analysis of the expectation values of the coupled tensors $w_0^{(ab)r}$ for an LSJ-coupled ground state is given in Ap-

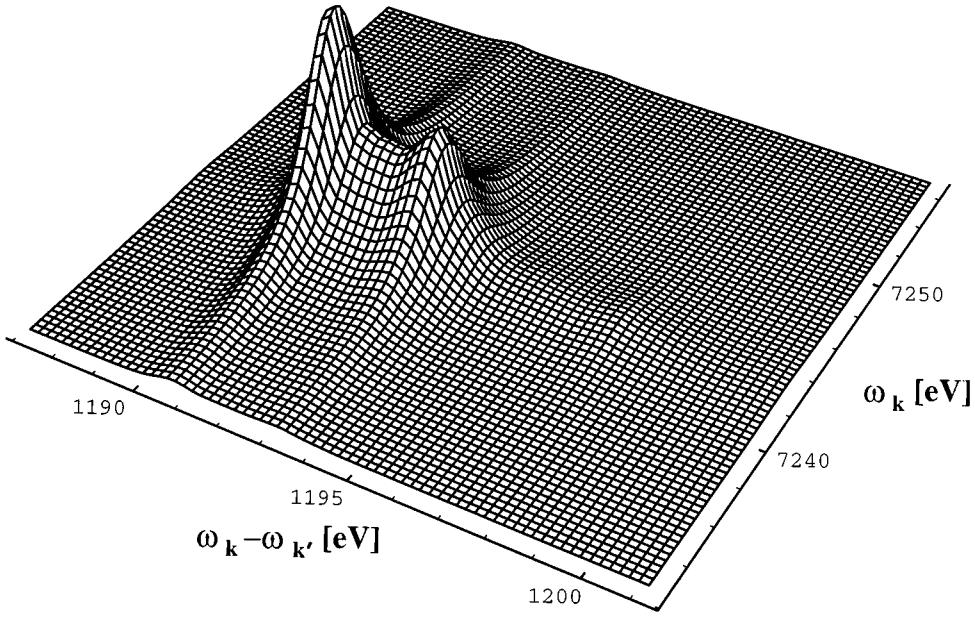

FIG. 3. Calculation of the resonant Raman spectrum of Gd^{3+} as a function of excitation energy $\omega_{\mathbf{k}}$ and transferred energy $\omega_{\mathbf{k}} - \omega_{\mathbf{k}'}$. Only the $L_3 M_5$-edge spectrum is displayed.

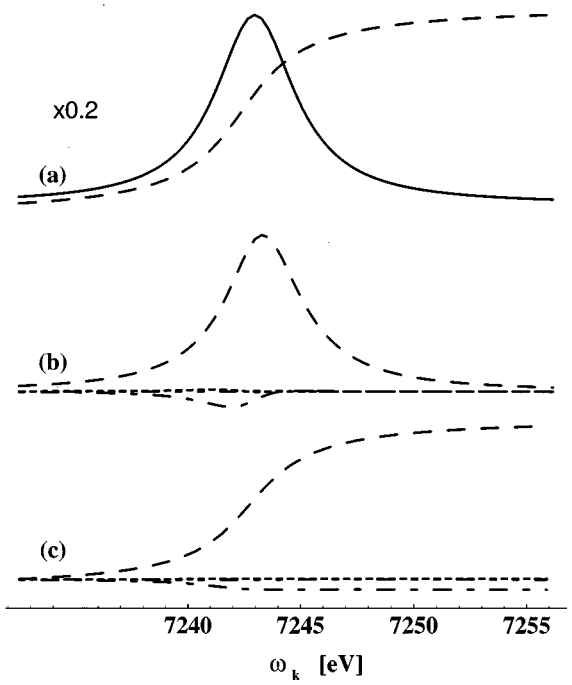

FIG. 4. Gd^{3+} spectra integrated along the $\omega_{\mathbf{k}}-\omega_{\mathbf{k}'}$ axis. From top to bottom: (a) Numerical evaluation of $I^{(00)0}$ (solid line); the dashed line gives the integral of the solid line along the $\omega_{\mathbf{k}}$ axis. The integrated intensity is normalized so that the maximum of the isotropic integrated spectrum corresponds to the maximum height of the peak. Notice the scaling. (b) Calculation of $I^{(10)1}$ (dashed line), $I^{(20)2}$ (dash-dotted line), $I^{(30)3}$ (dotted line), and $I^{(40)4}$ (dash-dot-dotted line). (c) The curves given in (b) integrated along the $\omega_{\mathbf{k}}$ axis.

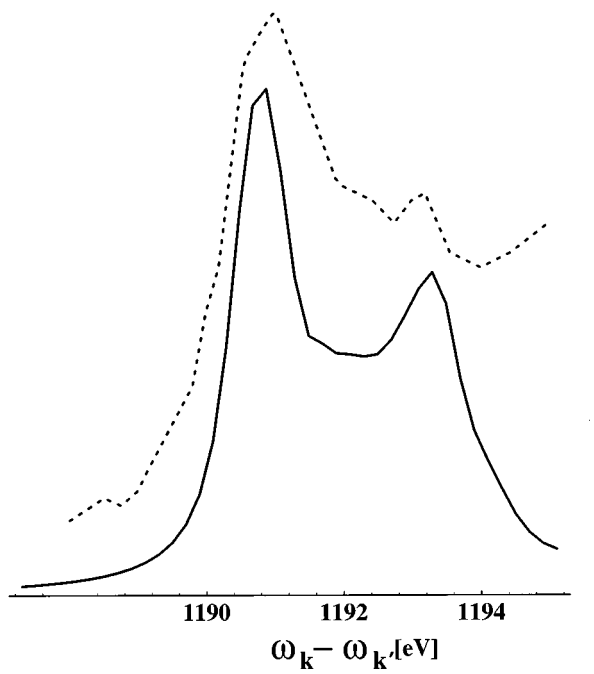

FIG. 5. Comparison between the calculated resonant Raman spectrum and the experimental data of Krisch *et al.*, at the resonance energy: $\omega_{\mathbf{k}}=7243$ eV.

pendix B. A comparison with the values obtained for trivalent rare-earth ions shows that LSJ coupling gives a good agreement for spin-independent operators. For spin-dependent operators trends along the rare-earth series are well described.

Intensities integrated from $-\infty$ to ω_1 are depicted in Fig. 4(c). Notice that a vanishing integrated intensity does not necessarily imply a vanishing spectrum; normally, however, if the integral over a spin-orbit split edge is small, the spectrum has low intensity at that edge.

For $\omega_1=7243$ eV, the numerical results are compared to the experimental data[24] in Fig. 5. The good agreement provides further evidence for the quadrupolar nature of the pre-edge structure.

B. Dysprosium, holmium, and erbium

This section briefly discusses numerical results for Dy^{3+} ($4f^9$ ground state, $^6H_{15/2}$), Ho^{3+} ($4f^{10}$, $^5I_8$), and Er^{3+} ($4f^{11}$, $^4I_{15/2}$). The unpolarized spectra are depicted in Figs. 6, 8, and 10, respectively. By comparing them to $3d\rightarrow 4f$ x-ray absorption spectra significant differences emerge.

For polarized ingoing radiation the integrated spectra are displayed in Figs. 7, 9, and 11. In the spectra of part (c) of the figures the value of a given $I^{(z0)z}$, at an energy $\omega_{\mathbf{k}}$ well above the $2p_{3/2}$ threshold, is expressible as a linear combination of expectation values $\langle w_0^{(ab)r}\rangle$. Ingoing-photon circular dichroism selects an angle-dependent linear combination of $I^{(10)1}$ and $I^{(30)3}$ (analogous to the case of $2p$ x-ray circular dichroism). As a function of $\cos\theta$, with θ the angle between the direction of the incoming light and the magnetization axis, $I^{(10)1}$ and $I^{(30)3}$ behave like Legendre polynomials of order 1 and 3, respectively.

V. CONCLUSION

Working within the framework of a single-ion model, this paper has developed a theory of XRRS in the rare earths. A symmetry analysis of the resonance has been presented; extensive numerical calculations have also been discussed and compared with recent experimental data.

The symmetry analysis provides a poweful tool for disentangling the large variety of polarization responses stemming from a two-photon process. As a result of a coupled-multipolar expansion, the scattering cross section is expressed as a linear combination of pairs of tensors of increasing rank; each pair consists of a polarization response (the angular dependence) and the ground-state expectation value of a frequency-dependent operator (the electronic transition), coupled together to give a scalar. For a given experimental setup, the contributions to the scattered intensity can then be determined in any point-group symmetry. Particularly simple expressions are obtained in the case of ingoing and/or outgoing isotropic radiation. Furthermore, the integrated intensity can be conveniently factorized into an excitation and a deexcitation components.

Full-multiplet calculations in cylindrical symmetry have been reported for the resonance $2p\rightarrow 4f$, $3d\rightarrow 2p$ in the rare-earth ions Gd^{3+}, Dy^{3+}, Ho^{3+}, and Er^{3+}. Combined with the results of the symmetry analysis, these calculations can provide a good description of the integrated intensities,

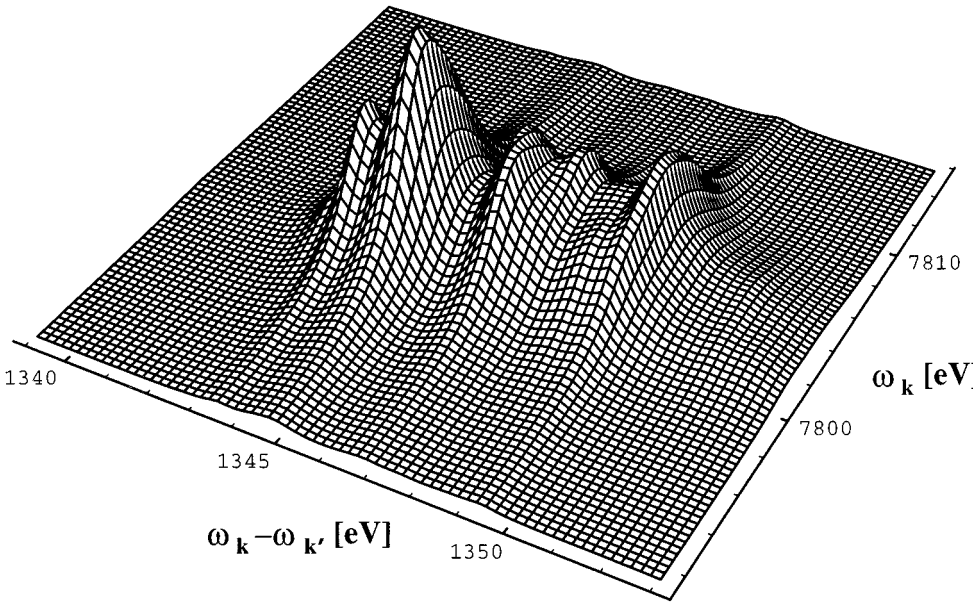

FIG. 6. Calculation of the resonant Raman spectrum of Dy^{3+} as a function of excitation energy $\omega_{\mathbf{k}}$ and transferred energy $\omega_{\mathbf{k}}-\omega_{\mathbf{k}'}$. Only the L_3M_5-edge spectrum is displayed.

as shown by the agreement between our Gd^{3+} spectra and the data recorded by Krisch and co-workers, using isotropic ingoing and outgoing radiation. In this case, the quadrupolar nature of the pre-edge part of the spectrum is confirmed.

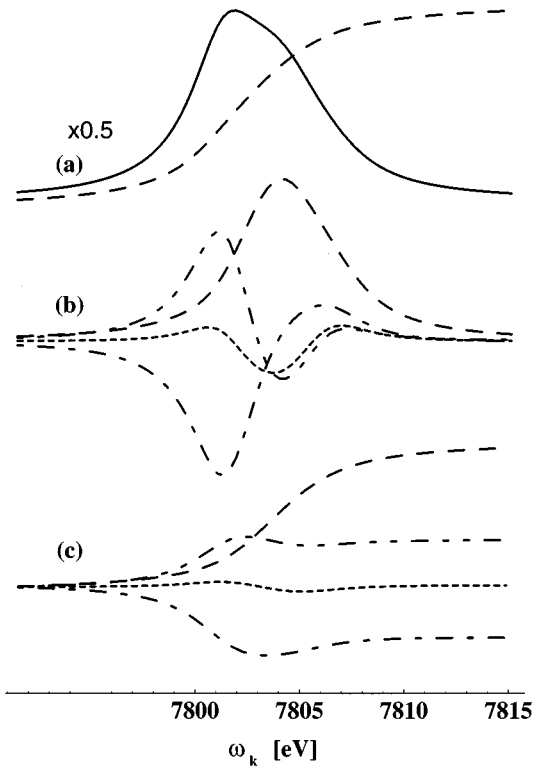

FIG. 7. Dy^{3+} spectra integrated along the $\omega_{\mathbf{k}}-\omega_{\mathbf{k}'}$ axis. The curves are depicted according to the caption of Fig. 4.

ACKNOWLEDGMENTS

We are grateful to B. N. Harmon for correspondence. M.V. acknowledges financial support from the European Union.

APPENDIX A

This appendix provides a short summary of results for nj symbols.

A $3j$ symbol with two equal quantum numbers can be written as

$$\begin{pmatrix} l & a & l \\ -\lambda' & \alpha & \lambda \end{pmatrix} = \frac{r_{la}(\lambda'\alpha\lambda)}{r_{la}} n_{la} = \overline{r_{la}}(\lambda'\alpha\lambda) n_{la}$$

$$\xrightarrow{\alpha=0} \frac{r_{la}(\lambda)}{r_{la}} n_{la} = \overline{r_{la}}(\lambda) n_{la}. \qquad \text{(A1)}$$

($3j$ symbols of this kind appear in the definition of tensors acting on a single atomic shell.) Using the definition of n_{la}, Eq. (24), we have

$$r_{la} = r_{la}(l) = \frac{1}{2^a} \frac{(2l)!}{(2l-a)!}, \qquad \text{(A2)}$$

so that $\overline{r_{la}}(l0l)=1$. $r_{la}(\lambda'\alpha\lambda)$ and $\overline{r_{la}}(\lambda'\alpha\lambda)$ appear therefore as naturally defined $3j$ symbols. Setting $a=1$, we find

$$r_{l1}(\lambda' q\lambda) = \langle l\lambda'|L_q|l\lambda\rangle; \qquad \text{(A3)}$$

in a similar way, $r_{\frac{1}{2}1}(\sigma' q\sigma)$ provides the matrix element of S_q. When $q=0$, the matrix element is fully determined by $r_{la}(\lambda)$; notice that these functions

$$r_{l0}(\lambda) = 1,$$

$$r_{l1}(\lambda) = \lambda,$$

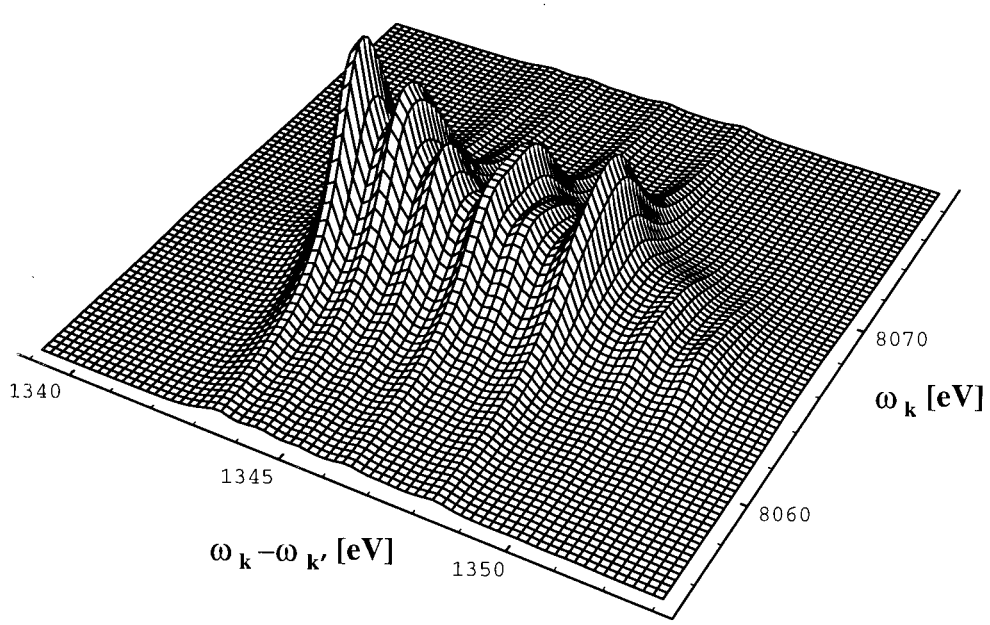

FIG. 8. Calculation of the resonant Raman spectrum of Ho^{3+} as a function of excitation energy $\omega_{\mathbf{k}}$ and transferred energy $\omega_{\mathbf{k}}-\omega_{\mathbf{k}'}$. Only the L_3M_5-edge spectrum is displayed.

$$r_{l2}(\lambda)=\tfrac{1}{2}(3\lambda^2-\boldsymbol{l}^2),$$

$$r_{l3}(\lambda)=\tfrac{1}{2}[5\lambda^2-3\lambda(\boldsymbol{l}^2-\tfrac{1}{3})],$$

with $\boldsymbol{l}^2=l(l+1)$, bear a strong resemblance to the Legendre polynomials.

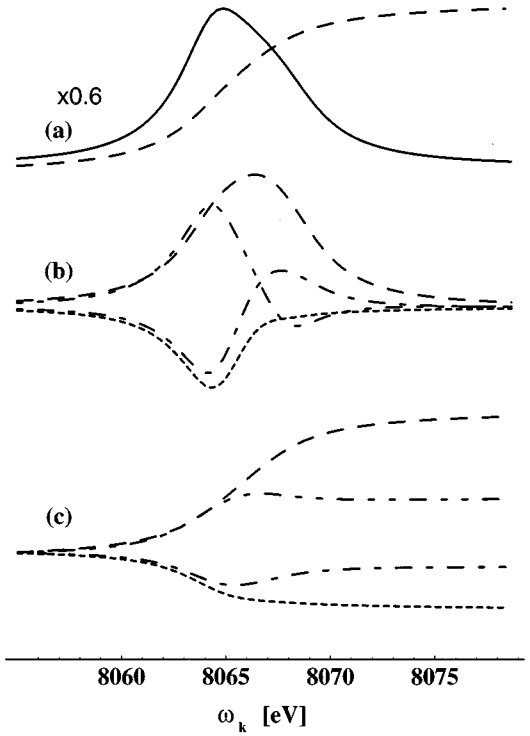

FIG. 9. Ho^{3+} spectra integrated along the $\omega_{\mathbf{k}}-\omega_{\mathbf{k}'}$ axis. The curves are depicted according to the caption of Fig. 4.

$6j$ and $9j$ symbols with degenerate triads can be reduced by use of the normalization constants n_{la} and n_{abr}. [n_{abr} is defined by Eq. (25).] The present work implements the reduction formulas

$$\begin{Bmatrix} j & j & x \\ j' & j' & J \end{Bmatrix} = \begin{cases} (-)^{2j+2j'} n_{jx} n_{j'x}, & \text{if } J=j+j', \\ (-)^{2j_>+x} \dfrac{n_{j_<x}}{[j_>]n_{j_>x}}, & \text{if } J=|j-j'|, \end{cases} \tag{A4}$$

and

$$\begin{Bmatrix} j & j & a \\ j' & j' & b \\ j+j' & j+j' & c \end{Bmatrix} = (-)^{a+b} \frac{n_{ja} n_{j'b}}{[j+j']n_{j+j'c}} n_{abc}, \tag{A5}$$

where $j_<$ and $j_>$ denote the smaller and greater value of j and j', respectively.

APPENDIX B

This appendix reports analytical results for $\langle w_0^{(ab)r} \rangle$ for a Hund's rule ground state.

Consider the matrix element

$$\langle LSJM_J|w_0^{(ab)r}|LSJM_J\rangle = \langle LSJM_J|[v^a t^b]_0^r|LSJM_J\rangle n_{abr}^{-1}, \tag{B1}$$

with the tensor coupling to a total r defined by Eq. (2). The application of the Wigner-Eckart theorem, followed by a recoupling, yields

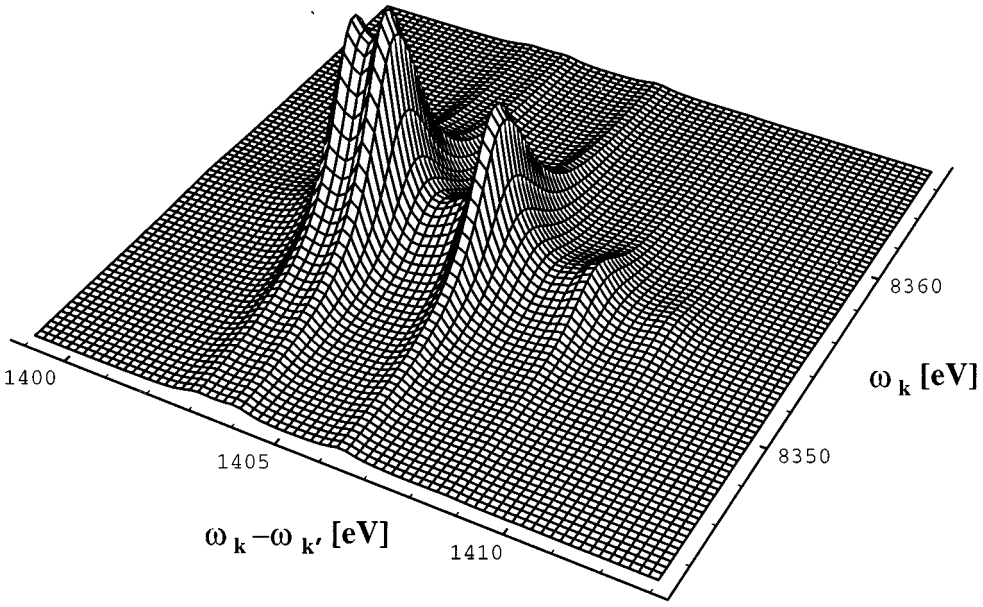

FIG. 10. Calculation of the resonant Raman spectrum of Er^{3+} as a function of excitation energy $\omega_{\mathbf{k}}$ and transferred energy $\omega_{\mathbf{k}}-\omega_{\mathbf{k}'}$. Only the L_3M_5-edge spectrum is displayed.

$$\langle LSJM_J|w_0^{(ab)r}|LSJM_J\rangle = [J](-1)^{J-M_J} n_{abr}^{-1} \begin{pmatrix} J & r & J \\ -M_J & 0 & M_J \end{pmatrix} \times \begin{Bmatrix} L & L & a \\ S & S & b \\ J & J & r \end{Bmatrix} \langle L\|v^a\|L\rangle\langle S\|t^b\|S\rangle. \quad \text{(B2)}$$

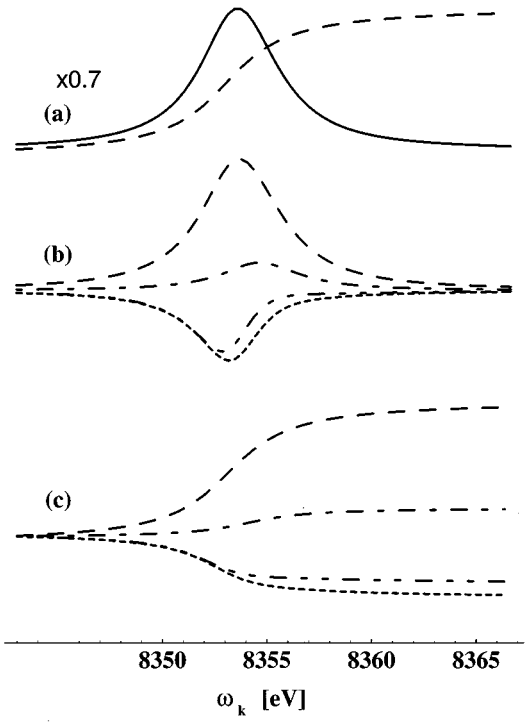

FIG. 11. Er^{3+} spectra integrated along the $\omega_{\mathbf{k}}$-$\omega_{\mathbf{k}'}$ axis. The curves are depicted according to the caption of Fig. 4.

The reduced matrix elements are determined as follows. Given the one-electron matrix elements v^a and t^b,

$$\langle l\lambda|v_0^a|l\lambda\rangle = \overline{r_{la}}(\lambda),$$

$$\langle \tfrac{1}{2}\sigma|t_0^b|\tfrac{1}{2}\sigma\rangle = \overline{r_{(1/2)b}}(\sigma), \quad \text{(B3)}$$

with $\overline{r_{la}}$ defined in the preceding appendix, consider the state $|L,M=L\rangle$. The matrix element of v^a becomes

$$\langle LL|v_0^a|LL\rangle = \sum_\lambda \overline{r_{la}}(\lambda), \quad \text{(B4)}$$

where the holes (or electrons) contained in $|LL\rangle$ are labeled by l and λ. [More(less)-than-half-filled shells are described in terms of holes (electrons).] On the other hand, the Wigner-Eckart theorem yields

$$\langle LL|v_0^a|LL\rangle = \begin{pmatrix} L & a & L \\ -L & 0 & L \end{pmatrix} \langle L\|v^a\|L\rangle. \quad \text{(B5)}$$

Combining Eqs. (B4) and (B5), we have

$$\langle L\|v^a\|L\rangle = n_{La}^{-1} \sum_\lambda \overline{r_{la}}(\lambda). \quad \text{(B6)}$$

The reduced matrix element of t^b is obtained in a similar way.

Setting $M_J=J$ in Eq. (B2) to obtain a magnetic ground state and applying the $9j$-symbol-reduction formula of Appendix A, we find

$$\langle LSJJ|w_0^{(ab)r}|LSJJ\rangle = F_{JL}^{ar} \sum_\lambda \overline{r_{la}}(\lambda), \quad \text{(B7)}$$

where

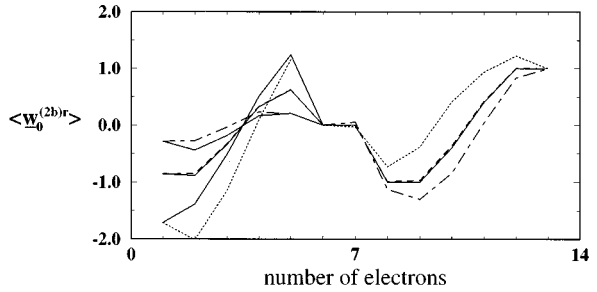

FIG. 12. Ground-state expectation values of coupled tensor operators $\langle w_0^{(2b)r}\rangle$. The solid lines give their values in LSJ coupling. Dashed lines are the values calculated for trivalent rare-earth atoms, where the dashed line gives $\langle w_0^{(20)2}\rangle$, the dotted line $\langle w_0^{(21)1}\rangle$, and the dash-dotted line $\langle w_0^{(21)3}\rangle$. The related $\langle w_0^{(ab)r}\rangle$ in LSJ coupling are those that are equal for $n=1$.

$$F_{JL}^{ar}=\begin{cases} -\dfrac{[J]n_{Jr}^2}{[L]n_{La}^2}, & J=L-S,\ \ \lambda=-3,-2,-1,\ldots, \\ \\ 1 & J=L+S,\quad \lambda=3,2,1,\ldots, \end{cases} \tag{B8}$$

that is, the matrix element (B2) expressed as a sum of expectation values of the one-particle operator v^a. The function F_{JL}^{ar} accounts for the coupling of L and S to a total J; the summation over λ must be performed as indicated. (The matrix elements of t^b are diagonal.)

In simple cases, well-known results are recovered. Given $L_z=-lw_0^{(10)1}$, we have $l\Sigma_\lambda \overline{r_{l1}}(\lambda)=\Sigma_\lambda \lambda=L$, so that

$$\langle L_z\rangle=-l\langle w_0^{(10)1}\rangle=\begin{cases} -\dfrac{J(L+1)}{J+1} & J=L-S, \\ \\ -L & J=L+S, \end{cases} \tag{B9}$$

that is, the expression obtainable by setting $J=J_z=L\pm S$ in Landé's formula. Also, given $S_z=-sw_0^{(01)1}$, we have $s\Sigma_\lambda \overline{r_{l0}}(\lambda)=s\Sigma_\lambda 1=S$, so that

$$\langle S_z\rangle=-s\langle w_0^{(01)1}\rangle=\begin{cases} \dfrac{JS}{J+1} & J=L-S, \\ \\ -S & J=L+S. \end{cases} \tag{B10}$$

In LSJ coupling, spin enters the matrix element via Eq. (B8). As a result, $\langle w_0^{(ab)r}\rangle$ is b and r independent, for a more-than-half-filled shell; a specific example, $\langle w_0^{(2b)r}\rangle$, of this behavior is depicted in Fig. 12. (Spin-independent operators are accurately described by LSJ coupling; for spin-dependent ones deviations are found, as the spin-orbit coupling mixes in other J values.)

*Also at Department of Chemical Physics, Materials Science Centre, University of Groningen, Nijenborgh 16, 9747 AG Groningen, The Netherlands.

[1] J. K. Lang, Y. Baer, and P. A. Cox, J. Phys. F **11**, 121 (1981).
[2] B. T. Thole, G. van der Laan, J. C. Fuggle, G. A. Sawatzky, R. C. Karnatak, and J.-M. Esteva, Phys. Rev. B **32**, 5107 (1985).
[3] In general, treating the very local $4f$ states as bands results in noninteger occupation of $4f$ levels and the pinning of the $4f$-band complex at the Fermi level. Even in gadolinium, where the exchange splitting results in the seven occupied spin-up states being placed well below the Fermi level, the $4f$ spin-down states are positioned too low in energy and appear just above the Fermi level. Methods to correct the problem of treating rare earths include the so-called LDA+U (local density approximation with on-site Coulomb repulsion) prescription, where the $4f$ states are handled within a Hartree-Fock-like formalism with the intra-atomic Coulomb and exchange integrals explicitly evaluated.
[4] G. Schütz, M. Knülle, R. Wienke, W. Wilhelm, W. Wagner, P. Kienle, and R. Frahm, Z. Phys. B **73**, 67 (1988).
[5] P. Carra and M. Altarelli, Phys. Rev. Lett. **64**, 1286 (1990).
[6] P. Carra, B. N. Harmon, B. T. Thole, M. Altarelli, and G. A. Sawatzky, Phys. Rev. Lett. **66**, 2495 (1991).
[7] X. D. Wang, T. C. Leung, B. N. Harmon, and P. Carra, Phys. Rev. B **47**, 9087 (1993).
[8] J. C. Lang, G. Srajer, C. Detlefs, A. I. Goldman, H. König, X. Wang, B. N. Harmon, and R. W. McCallum, Phys. Rev. Lett. **74**, 4935 (1995).
[9] K. Hämäläinen, D. P. Siddons, J. B. Hastings, and L. E. Berman, Phys. Rev. Lett. **67**, 2850 (1991).
[10] P. Carra, M. Fabrizio, and B. T. Thole, Phys. Rev. Lett. **74**, 3700 (1995).
[11] B. T. Thole, P. Carra, F. Sette, and G. van der Laan, Phys. Rev. Lett. **68**, 1943 (1992).
[12] P. Carra, B. T. Thole, M. Altarelli, and X. Wang, Phys. Rev. Lett. **70**, 694 (1993).
[13] A. I. Akhiezer and V. B. Berestetsky, *Quantum Electrodynamics* (Consultants Bureau, New York, 1957).
[14] A. P. Yutsis, I. B. Levinson, and V. V. Vanagas, *Mathematical Apparatus of the Theory of Angular Momentum* (Israel Program for Scientific Translation, Jerusalem, 1962).
[15] D. A. Varshalovich, A. N. Moskalev, and V. K. Khersonskii, *Quantum Theory of Angular Momentum* (World Scientific, Singapore, 1988).
[16] B. R. Judd, *Second Quantization in Atomic Spectroscopy* (Johns Hopkins University Press, Baltimore, 1967).
[17] J. Luo, G. T. Trammell, and J. P. Hannon, Phys. Rev. Lett. **71**, 287 (1993).
[18] P. Carra and M. Fabrizio, in *Core Level Spectroscopies for Magnetic Phenomena: Theory and Experiment*, edited by P. S. Bagus *et al.* (Plenum Press, New York, 1995).
[19] B. T. Thole and G. van der Laan, Phys. Rev. Lett. **70**, 2499 (1993).
[20] B. T. Thole and G. van der Laan, Phys. Rev. B **49**, 9613 (1994).
[21] B. T. Thole, G. van der Laan, and M. Fabrizio, Phys. Rev. B **50**, 11 466 (1994).
[22] P. Carra, H. König, B. T. Thole, and M. Altarelli, Physica B **192**, 182 (1993).
[23] P. Carra and B. T. Thole, Rev. Mod. Phys. **66**, 1509 (1994).
[24] M. H. Krisch, C. C. Kao, F. Sette, W. A. Caliebe, K. Hämäläinen, and J. B. Hastings, Phys. Rev. Lett. **74**, 4931 (1995).
[25] R. D. Cowan, *The Theory of Atomic Structure and Spectra* (University of California Press, Berkeley, 1981).
[26] P. H. Butler, *Point Group Symmetry, Applications, Methods and Tables* (Plenum, New York, 1981).